

# Sensor Management In 2D Lidar Based Underground Positioning

Kristin Nielsen and Gustaf Hendeby

The self-archived postprint version of this journal article is available at Linköping University Institutional Repository (DiVA):

<http://urn.kb.se/resolve?urn=urn:nbn:se:liu:diva-167482>

N.B.: When citing this work, cite the original publication.

Nielsen, K., Hendeby, G., (2020), Sensor Management In 2D Lidar Based Underground Positioning, *Proceedings 2020 IEEE 23rd International Conference on Information Fusion (FUSION)*, , 765-772. <https://doi.org/10.23919/FUSION45008.2020.9190382>

Original publication available at:

<https://doi.org/10.23919/FUSION45008.2020.9190382>

Copyright: Institute of Electrical and Electronics Engineers (IEEE)

<http://www.ieee.org/>

©2020 IEEE. Personal use of this material is permitted. However, permission to reprint/republish this material for advertising or promotional purposes or for creating new collective works for resale or redistribution to servers or lists, or to reuse any copyrighted component of this work in other works must be obtained from the IEEE.



# Sensor Management in 2D Lidar-Based Underground Positioning

Kristin Nielsen<sup>\*†</sup> and Gustaf Hendeby<sup>†</sup>

<sup>\*</sup>Rocktec Automation; Epiroc Rock Drills AB; Örebro, Sweden

kristin.nielsen@epiroc.com

<sup>†</sup>Dept. Electrical Engineering; Linköping University; Linköping, Sweden

gustaf.hendeby@liu.se

**Abstract**—Lidar-based positioning in a 2D map is analyzed as a method to provide a robust, high accuracy, and infrastructure-free positioning system required by the automation development in underground mining. Expressions are derived that highlight separate information contributions to the obtained position accuracy. This is used to develop two new methods that efficiently select which subset of available lidar rays to use to reduce the computational complexity and allow for online processing with minimal loss of accuracy. The results are verified in simulations of a mid-articulated underground loader in a mine. The methods are shown to be able to reduce the number of rays needed without considerably affecting the performance, and to be competitive with currently used methods. Furthermore, simulations highlight the effects of errors in the map and other map properties, and how imperfect maps degrades the performance of different selection strategies.

**Index Terms**—underground positioning, sensor management, sensor selection, lidar, mine localization

## I. INTRODUCTION

Up until today, the majority of positioning systems available in underground mines have focused on personal safety and emergency rescue, where knowledge of who is in the mine and at what level is enough [1]. However, a real-time, highly accurate positioning system would have the potential to significantly improve safety for present human workers, contribute to the advancement of automated vehicle systems, and enable the deployment of productivity improving fleet management systems for underground operations. [2].

Today, autonomous operation in underground mines is possible for specific tasks and preconditions, *e.g.*, loaders navigating along prerecorded paths are commercially available from Sandvik, Caterpillar, and Epiroc [3]. These systems rely on laser scanners, odometry, and *inertial measurement units* (IMUs) to solve their tasks. These applications do not require global positioning due to prerecording of the environment.

Dead reckoning based localization, using IMUs and odometry, is a favorable solution as it requires no external infrastructure and is robust to the dirty mine environment. However, it inherently suffers from drift [4] and cannot be used alone for extended periods of time, but is an important component when fused with other information sources [1, 5].

This work was partially supported by the Wallenberg AI, Autonomous Systems and Software Program (WASP) funded by the Knut and Alice Wallenberg Foundation.

WiFi network [6], RFID [7, 8], and *ultra wideband* (UWB) [1, 9, 10] based methods are often put forward for indoor positioning. WiFi and RFID have been reported to provide meter accuracy in office environments, but dust and fog as well as roughness and irregularities in the walls distinguish the underground environment from the indoor scenario. Attempts with WiFi based positioning in underground environments reports lower accuracy [11, 12]. UWB is a promising technology due to its high precision (15 cm reported indoors [13]). However, metallic objects can cause disturbances [7] and sensitivity to optimal placement of the UWB anchors [14] limits the applicability in mines.

Another possible method is to compare lidar measurements to a map [15]. This has been used with good results indoors, and uses the same sensors as existing commercial autonomous mine solutions have. Hence, this is the solution pursued in this paper, taking into account the availability of accurate maps and limited computing power.

The environment in an underground mine changes dynamically as the result of tunnels being extended, falling rocks, and wall reinforcements. Accurate map creation is considered in [2]. In this paper the map is assumed known beforehand, and the effects of map inaccuracies are considered in the analysis and evaluation.

Lidars typically produce a high number of measurements to process. The loader considered in this paper features two 2D lidars, each covering 180° and with a resolution of 1° at 20 Hz and in the future 3D lidars with higher update rates are to be expected resulting in even larger amounts of measurements. Hence, methods to limit the computations, without losing quality are necessary to achieve real time performance. This leads to the sensor selection problem studied in this paper.

The sensor selection problem is a well-known topic [16, 17] and can be formulated as an optimization problem. In this particular case, to choose which individual lidar rays to process to maximize the accuracy in the position estimate. In general the optimization problem is computationally expensive to solve. Convex relaxations [18, 19] can simplify, but the problem is still too complex to be solved in real time. Greedy, but sub-optimal, approaches are therefore often used. They requires a proxy of the quality measure that is sub-modular to guarantee optimality [20]. The *mean square error* (MSE) as a performance measure is not sub-modular, but often still

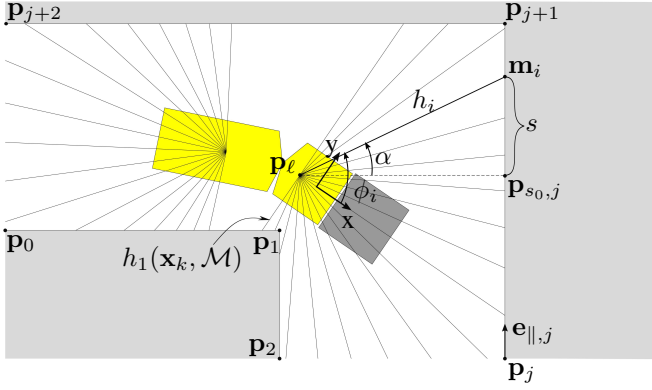


Fig. 1. An articulated vehicle with one lidar mounted at the front part of the vehicle and one at the rear part. The origin of the sensor fixed coordinate system is the point in the middle of the front wheel axis. The thin lines represent a subset of available laser rays.

performs well in simulations [21, 22].

This paper studies the problem of positioning a loader in an underground mine with help of lidar measurements and a 2D map of the environment. The contributions are the following:

- A thorough analysis of the information available in the lidar measurements. Expressions are derived, in which the contributions to the information are separated into contributions related to the map and to the pose of the vehicle.
- Two different greedy methods to approximate the solution to the sensor selection problem. One based on an analysis of the map, and one studying the obtained measurements. Both based on the analysis of the information content.
- Simulation studies to evaluate the properties of the theoretical results.

This paper is structured as follows. First in Sec. II the estimation problem, the map representation, and a solution given lidar measurements are presented. The information available from the measurements is analyzed in Sec. III, and based on this, solutions to the sensor selection problem are derived in Sec. IV. The methods are then evaluated in Sec. V before concluding remarks are given in Sec. VI.

## II. POSITIONING SOLUTION

The pose of the considered mid-articulated loader is estimated using an *unscented Kalman filter* (UKF) which combines measured odometry and IMU data with how well lidar measurements fit the map. As illustrated in Fig. 1, the pose at time  $k$ ,  $\mathbf{x}_k = [x_k, y_k, \theta_k]^T$ , comprise the Cartesian position  $(x_k, y_k)$  in the map reference, and the heading  $\theta_k$ . The articulation of the loader is assumed known.

### A. Dynamic Model

The motion of the loader can be predicted based on odometry and IMU measurements as

$$\mathbf{x}_{k+1} = \begin{bmatrix} x_k + v_k \cos \theta T \\ y_k + v_k \sin \theta T \\ \theta_k + \dot{\theta}_k T \end{bmatrix} + u_k, \quad (1)$$

where the speed  $v_k$  comes from the odometry, the change of heading  $\theta_k$  from the gyroscope in the IMU, and  $T$  is the sample time. The process noise,  $u_k$ , captures the errors in the measured motion. It is assumed to be Gaussian white noise,  $u_k \sim \mathcal{N}(0, \mathbf{Q}_k)$ .

The process noise includes errors from the odometry, predominately stemming from wheel slip and skidding, and noise in the IMU measurements, introduced by vibrations. These factors, which might vary between scenarios depending on properties of the mine environment, determine the noise levels to use. For example, some wheel slip will almost certainly occur during bucket loading. Underground loaders typically has the capacity to transport 10–20 tonnes of raw material in their buckets. A filled/empty bucket will influence the dynamics of the vehicle, which has to be accounted for by the noise level.

### B. Lidar Measurements

The predicted pose is corrected by using the distance to the mine walls, measured by the lidars mounted on the loader, as illustrated in Fig. 1. Each lidar covers  $180^\circ$  with a distance measurement each degree. The resulting measurements can mathematically be described by

$$\mathbf{y}_k = \begin{bmatrix} h_1(\mathbf{x}_k, \mathcal{M}) \\ h_2(\mathbf{x}_k, \mathcal{M}) \\ \vdots \\ h_K(\mathbf{x}_k, \mathcal{M}) \end{bmatrix} + e_k, \quad (2)$$

where  $\mathbf{y}_k$  is a vector of measured ranges for each individual laser ray at time step  $k$ ,  $\mathcal{M}$  represents the map, and  $e_k$  is the measurement noise which is assumed white and Gaussian,  $e_k \sim \mathcal{N}(0, \mathbf{R}_k)$ .

Each laser ray  $i$  gives rise to

$$h_i(\mathbf{x}_k, \mathcal{M}) = \|\mathbf{m}_i - \mathbf{x}_k\|, \quad i = 1, \dots, K, \quad (3)$$

the distance to the wall in the direction of the  $i$ th ray, and where  $\mathbf{m}_i$  is the point in the map where the laser ray will hit the wall. Hence,  $\mathbf{m}_i$  is a function of the map  $\mathcal{M}$  and the pose of the loader. The point  $\mathbf{m}_i$  can, e.g., be determined using ray casting.

The error in the lidar measurements originates mainly from four sources:

- Errors in the map.
- Errors due to the assumption of a planar 2D world. The lidars are mounted at a fixed height and since the ground where the vehicle is driving is not perfectly planar, the roll and pitch of the vehicle will make the laser ray hit a different vertical spot on the wall than intended. This adds errors especially for long range measurements due to the angle of the measurement.
- Errors from the underlying physics of the lidar. At large ranges the rays become cone shaped. This makes the error depend on the range of the measurement and also the inclination angle of the ray to the wall. [23]

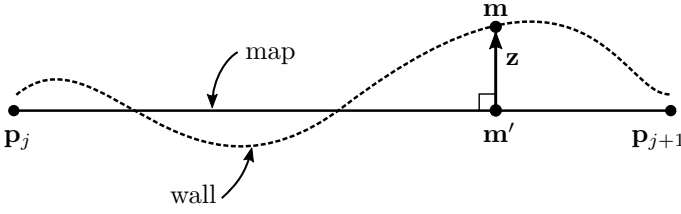


Fig. 2. The error in a map can be described by the perpendicular disturbance  $\mathbf{z}$  in a point  $\mathbf{m}'$  in the map.

- Errors from the articulation angle sensor, which causes the ray to be cast in a different direction than expected, resulting in the wrong distance being measured.

For simplicity, the measurement noise in each direction can be assumed independent, resulting in a diagonal covariance matrix  $\mathbf{R}_k$ .

### C. Map Representation

The predefined 2D map consists of line segments put together to build up the wall structure of the area of operation seen from above, see Fig. 1. The map,  $\mathcal{M}$ , is represented by a set of corner points,

$$\mathcal{M} = \{\mathbf{p}_0, \mathbf{p}_1, \dots, \mathbf{p}_n\}, \quad (4)$$

listed in a counter clockwise manner. The straight line segments

$$\ell_j = \mathbf{p}_{j+1} - \mathbf{p}_j, \quad (5)$$

connecting the points represent the walls. Any points on a wall segment can be parametrized as

$$\mathbf{m} = \mathbf{p}_{s_0, j} + s \mathbf{e}_{\parallel, j}, \quad (6)$$

with  $j \in [0, n-1]$ ,  $s$  as a scalar distance parameter,  $\mathbf{p}_{s_0, j}$  as the point on  $\ell_j$  where  $s = 0$  and

$$\mathbf{e}_{\parallel, j} = \frac{\mathbf{p}_{j+1} - \mathbf{p}_j}{\|\mathbf{p}_{j+1} - \mathbf{p}_j\|}. \quad (7)$$

A map can be acquired by a pre-mapping procedure where laser data is recorded either by the loader itself or by some other vehicle. Or, the map can be obtained from drawings made during the planning phase of the mine area. Both acquisition methods incorporate errors in the map due to the walls not being flat in the vertical direction, but also long straight tunnels drifting in direction. The former method will give a map with a more refined resolution of irregularities of the walls and the latter will give more conceptual maps with smoother walls.

The error in a map can be described as a perpendicular disturbance

$$\mathbf{z} = z \mathbf{e}_{\perp, j} \quad (8)$$

at a point  $\mathbf{m}'$  in the imperfect map, see Fig. 2. A point on the wall, or a point in a more accurate map, can then be written as

$$\mathbf{m} = \mathbf{m}' + \mathbf{z}. \quad (9)$$

### D. Unscented Kalman Filter

The *unscented Kalman filter* (UKF) [24] will be used to provide estimates of the pose of the loader. It is used as an approximation of the Kalman filter. The UKF approximation is suitable for problems where differentiating the motion and/or measurement model is hard, as it only relies on function evaluations. This is advantageous as the ray casting step in the measurement model is difficult to differentiate. See [25] for a complete derivation of the UKF. Implementation details can be found in [26, 27].

## III. INFORMATIVE SENSOR MEASUREMENTS

The sensor selection problem consists of finding the subset of lidar measurements that are as informative as possible with regard to the position estimate.

### A. Cramér-Rao Lower Bound

The *Cramér-Rao lower bound* (CRLB) provides a lower bound of the variance of any unbiased estimator of  $\mathbf{x}$ ,  $\text{cov}(\hat{\mathbf{x}}) \succeq \mathbf{I}^{-1}(\mathbf{x})$  where

$$\mathbf{I}(\mathbf{x}) = -\mathbb{E}_{\mathbf{y}}(\nabla_{\mathbf{x}}^2 \log p(\mathbf{x}, \mathbf{y})), \quad (10)$$

given mild regularity conditions [28].  $\mathbf{I}(\mathbf{x})$  is the *Fisher information matrix* (FIM) and information from independent measurements are additive

$$\mathbf{I}(\mathbf{x}) = \sum_{i=1}^K \mathbf{I}_i(\mathbf{x}). \quad (11)$$

The individual measurements in (3), each give rise to an information contribution

$$\mathbf{I}_i(\mathbf{x}) = \nabla_{\mathbf{x}}^T h_i(\mathbf{x}_k, \mathcal{M}) \mathbf{R}_i^{-1} \nabla_{\mathbf{x}} h_i(\mathbf{x}_k, \mathcal{M}). \quad (12)$$

Summing up the individual contributions yields the total information gained by one full lidar scan measurement. The remainder of this section outlines the different contributions to this information gain.

### B. Information in Lidar Measurements

First consider the derivative  $\nabla_{\mathbf{x}} h_i(\mathbf{x}_k, \mathcal{M})$  as defined in (3), where the arguments will be dropped to simplify the notation. A large value of this derivative will produce a large information contribution. The interpretation of it is the change in distance from the laser sensor to the wall, when the vehicle pose is perturbed. The chain rule yields

$$\nabla_{\mathbf{x}} h_i = \nabla_{\mathbf{r}} \|\mathbf{r}\| \nabla_{\mathbf{x}} (\mathbf{p}_{\ell}(\mathbf{x}) - \mathbf{m}_i(\mathbf{x}, \phi_i)). \quad (13)$$

where  $\mathbf{r} = \mathbf{m}_i - \mathbf{p}_{\ell}$ , and  $\mathbf{p}_{\ell}$  is the position of the laser sensor.

The first factor turns into a projection on the direction of the ray, given by the unit vector  $\mathbf{e}_{\phi_i}$ . This gives the first term

$$\nabla_{\mathbf{r}} \|\mathbf{r}\| \nabla_{\mathbf{x}} \mathbf{p}_{\ell} = \mathbf{e}_{\phi_i}^T ([\mathbf{I}^{2 \times 2} \quad \mathbf{0}^{2 \times 1}]), \quad (14)$$

which is interpreted as an information contribution in the direction of the ray that is always present independently of the map and the state.

Applying the chain rule again on the second term yields

$$-\mathbf{e}_{\phi_i}^T \nabla_{\mathbf{x}} \mathbf{m}_i = -\mathbf{e}_{\phi_i}^T \nabla_s \mathbf{m}_i \nabla_{\mathbf{x}} s = -\mathbf{e}_{\phi_i}^T \mathbf{e}_{\parallel,j} \nabla_{\mathbf{x}} s \quad (15)$$

where the last equality is from (6). This term describes how the vehicle position, relative the angle of the line segment, determines in what direction the measurement is informative. All scaled by the inclination angle of the laser ray to the line segment of the wall.

In total

$$\nabla_{\mathbf{x}} h_i = \mathbf{e}_{\phi_i}^T \left( [\mathbf{I}^{2 \times 2} \ \mathbf{0}^{2 \times 1}] - \mathbf{e}_{\parallel,j} \nabla_{\mathbf{x}} s \right), \quad (16)$$

which holds if the map is perfect without errors.

### C. Imperfect Map

Incorporate the error representation introduced by (8) and (9) yields

$$\nabla_{\mathbf{x}} h_i = \mathbf{e}_{\phi_i}^T \left( [\mathbf{I}^{2 \times 2} \ \mathbf{0}^{2 \times 1}] - \mathbf{e}_{\parallel,j} \nabla_{\mathbf{x}} s + \nabla_s z_i \mathbf{e}_{\perp,j} \nabla_{\mathbf{x}} s \right), \quad (17)$$

noticing that  $\mathbf{e}_{\parallel,j}$  and  $\mathbf{e}_{\perp,j}$  now refer to a line segment in the imperfect map. The contribution from this new third term to the state estimate, explains how errors in the map affect the position estimate. Assuming that the imperfect map is a smoother representation of the walls not capturing all irregularities, another interpretation is the influence of roughness of the wall on the information contribution. If the non-smoothness would be captured in the map, this term gives the information contribution by the small irregularities.

The information from one single laser ray can be calculated by,

$$\begin{aligned} \nabla_{\mathbf{x}}^T h_i \nabla_{\mathbf{x}} h_i &= \begin{bmatrix} \mathbf{e}_{\phi_i} \mathbf{e}_{\phi_i}^T & \mathbf{0}^{2 \times 1} \\ \mathbf{0}^{1 \times 2} & 0 \end{bmatrix} \\ &- \left( \mathbf{e}_{\phi_i}^T \mathbf{e}_{\parallel,j} + \nabla_s z_i \mathbf{e}_{\phi_i}^T \mathbf{e}_{\perp,j} \right) \left( \begin{bmatrix} \mathbf{e}_{\phi_i} \\ 0 \end{bmatrix} \nabla_{\mathbf{x}} s + \nabla_{\mathbf{x}} s^T \begin{bmatrix} \mathbf{e}_{\phi_i}^T & 0 \end{bmatrix} \right) \\ &+ \left( 1 + (\nabla_s z_i)^2 \right) \nabla_{\mathbf{x}} s^T \nabla_{\mathbf{x}} s, \quad (18) \end{aligned}$$

neglecting  $R_i^{-1}$  since it is just a scalar constant for an individual laser ray. As already mentioned  $\nabla_{\mathbf{x}} s$  explains the direction of the information contribution, this is then scaled by the inclination angle of the ray to the wall and by  $\nabla_s z_i$ .  $\nabla_s z_i$  is independent of the position of the vehicle and depends only on the map. Therefore in theory, it is possible to inspect only the map to find regions with a large potential of giving information measurements. Problems arise if the resolution of the irregularities are higher than the resolution of the sensor or the uncertainty of the positions, or if they are simply not included in the imperfect map.

The information contribution from a single laser ray is greater when the inclination angle is smaller, *i.e.*,  $\mathbf{e}_{\phi_i}$  is close to parallel to the wall. This is problematic since the uncertainty of the measurement increases at the same time due to the cone effect of the laser ray. It is therefore unreliable to maximize the information on this objective alone.

Using the geometry of the problem (see Fig. 1), an explicit expression for the parametrization of a line segment can be obtained

$$s = \frac{|\mathbf{p}_{s_0} - \mathbf{p}_\ell|}{\tan \alpha}, \quad (19)$$

where  $\alpha = \arccos(\mathbf{e}_{\parallel,i}^T \mathbf{e}_{\phi_i})$ . This yields the gradient

$$\begin{aligned} \nabla_{\mathbf{x}} s &= \frac{|\mathbf{p}_{s_0} - \mathbf{p}_\ell|}{\sin^2 \alpha} [0 \ 0 \ 1] \\ &- \frac{\cos \alpha}{\sin^2 \alpha} \begin{bmatrix} \mathbf{e}_{\phi_i}^T & 0 \end{bmatrix} + \frac{1}{\tan^2 \alpha} \begin{bmatrix} \mathbf{e}_{\parallel,i}^T & 0 \end{bmatrix} \end{aligned} \quad (20)$$

where the first term is the contribution in the heading direction of the vehicle, and the second and third terms is in the translational directions. Also here the problem with the contribution in each direction being greater when the inclination angle is small is present.

### D. Map Corner Points

Up until now, it is assumed that which line segment a laser ray hits is known. In close vicinity to the corner points  $\mathbf{p}_j$  this is uncertain. Here,  $\nabla_{\mathbf{x}} s$  is undefined and adopts different values if the corner is approached along  $\ell_j$  or  $\ell_{j+1}$ . The difference between the values depend on the angle between the two line segments and the inclination angle of the laser ray.

A large difference implies that the measurement is informative. Corners can be either convex or concave and a large angle between the line segments will in general increase the likelihood of getting informative measurements. But, how much this effect can be utilized depends on the inclination angle of the ray.

## IV. INFORMATIVE SENSOR SELECTION

Sec. III provides tools to offline analyze a map to gain knowledge about which regions of the map that will give particularly informative laser measurements. This section studies how the actual sensor selection can be performed with this knowledge in mind.

### A. Sensor Selection Problem

First let us introduce a sensor selection vector

$$\mathbf{w} = [w_1, w_2, \dots, w_M]^T \quad (21)$$

where each  $w_m \in \{0, 1\}$  and  $w_m = 1$  indicates that the  $m$ th laser measurement is selected. Using the additive property of the FIM allows for rewriting of (11) as

$$\mathbf{I}(x) = \sum_{m=1}^M w_m \mathbf{I}_m(x). \quad (22)$$

With a Bayesian approach the *a priori* error covariance can be taken into account [29], then the FIM can be decomposed into one part  $\mathbf{I}_D$ , from the obtained data, and one part  $\mathbf{I}_P$ , from the *a priori* error covariance,

$$\mathbf{I} = \mathbf{I}_D + \mathbf{I}_P = \sum_{m=1}^M w_m \mathbf{I}_m(\mathbf{x}) + \mathbf{I}_P. \quad (23)$$

By letting  $\mathbf{P}$  represent the *a priori* error covariance, assumed Gaussian, the expression for the FIM follows,

$$\mathbf{I} = \sum_{m=1}^M w_m \mathbf{I}_m(\mathbf{x}) + \mathbf{P}^{-1}. \quad (24)$$

Using the trace of the covariance matrix of the state estimate as a scalar performance measure, the sensor selection problem can be formulated as an optimization problem. Select  $K$  laser measurements out of the total  $M$  that minimizes the trace of the inverse FIM

$$\begin{aligned} & \text{minimize} && \text{tr} \left( \left[ \sum_{m=1}^M w_m \mathbf{I}_m(\mathbf{x}) + \mathbf{P}^{-1} \right]^{-1} \right) \\ & \text{subject to} && \mathbf{1}^T \mathbf{w} = k \\ & && w_m \in \{0, 1\}, \quad m = 1, \dots, M. \end{aligned} \quad (25)$$

Solving this optimization problem will give the best set of laser measurements in each measurement update; but it is not computationally feasible to solve, not even for rather small values of  $K$  and  $M$ . Below, three different sensor selection strategies are presented with this in mind.

### B. Uniformly Distributed (UNI)

The least computationally demanding and most straight forward strategy, is to select rays uniformly over the transmission angle. This strategy will be referred to as *uniformly distributed* (UNI). Every  $i$ th ray is selected and the result is sensitive to which ray chosen as starting index. No information about the map or the position of the vehicle is taken into consideration; but, this strategy is fast and computationally efficient. The UNI strategy is today used in applications where the computational resources are not enough to process all laser rays, and is therefore used as a benchmark in the experiments section.

### C. Greedy with Adjacent Rays (GAR)

A computationally feasible strategy is to solve the optimization problem with a greedy approach. Solve (25) for one measurement, fixate it in the set of selected measurements, and then again solve (25) with the remaining measurements. Continue iteratively until  $K$  measurements are selected. This method does not provide any optimality guarantees [21]. For the system of the mid-articulated loader, Fig. 3 shows how the CRLB decreases when the number of laser measurements used increases. Fig. 3 shows that the greedy approach is at least better than the UNI strategy.

Even though the greedy approach makes the problem feasible it is still too computationally heavy to perform online. If a point or region in the map is identified as informative, the selection strategy should make sure to capture that point/region even if the current position is uncertain. Therefore, it makes sense to select a burst of adjacent rays rather than selecting them one by one. Denote this strategy *greedy with adjacent rays* (GAR). Fig. 4 indicates that the information captured in a laser scan is very concentrated to only a few laser rays. A scan with 60 uniformly distributed rays is only as informative as 5 wisely chosen ones.

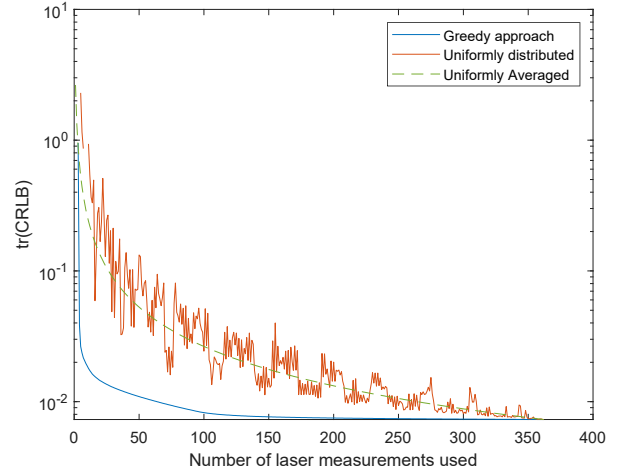


Fig. 3. The trace of the CRLB of the pose estimate when an increasing number of laser measurements are used. This is for Pose A in Fig. 5 in the realistic map (the blue one). The red line is for a single instance of the UNI strategy, and the dotted green line is when the UNI strategy is averaged over all possible starting index offsets of the transmission angle.

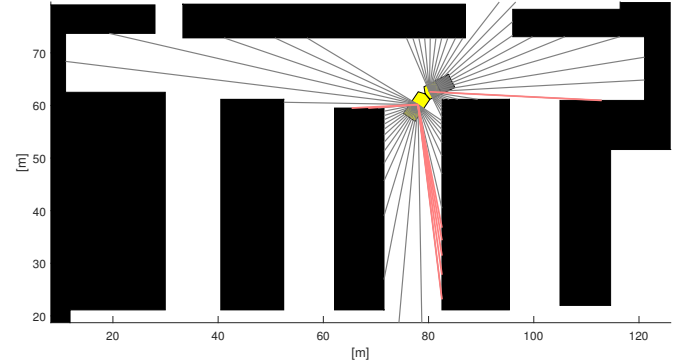


Fig. 4. For Pose D in Fig. 5 the trace of the CRLB is 0.0086 using 60 uniformly distributed rays. This is the black rays in the image. The 8 red laser rays are chosen according to the greedy approach, which yields only 0.0079 as the trace of the CRLB.

The selection strategy is then to first use the greedy approach to select a few laser rays, then add adjacent rays to compensate for the position uncertainty. If any of the first greedily selected rays are close to any other, there is a risk for selecting the same ray twice when adding adjacent rays. If that is the case, the algorithm will add more adjacent rays from one side.

### D. Local Difference in Measurement Data (LDM)

To cut the computational cost even more, a strategy is to consider only the observed lidar measurements, and assume that the properties of the map is incorporated in that data. This selection strategy will be referred to as *local difference in measurement data* (LDM). The idea is to compute the local difference in range between all adjacent pairs of laser rays, and then select the pairs that has a high difference. This corresponds to measurements where  $\nabla_{\mathbf{x}} s$ , and possibly also

$\nabla_s z$  are large in magnitude. Typically, a convex corner where the ray either hits or miss the wall will be selected. There is also a possibility that the high difference corresponds to only a large  $\nabla_s z$ . This could be a large irregularity or, if the map is not perfect, it could be an error in the map. In that case the selected measurement will give false information.

Due to the position uncertainty this strategy will select a few high-difference pairs, and then add adjacent rays. This strategy however, completely ignores in which direction ( $x$ ,  $y$ , or  $\theta$  in the state vector) the sensor measurement is informative. It will only find regions that has large  $\nabla_x s$  in magnitude, but the components of  $\nabla_x s$  are completely unknown. The first term in (18), tells us that a measurement always gives information in the aiming direction. At least for the Cartesian  $x$ ,  $y$  directions. To avoid a situation where all selected rays are informative in the same direction, this strategy spreads the aiming angles of the selected rays by splitting the observable half disc of each lidar into equally sized sections. In each section the ray pair with the largest difference is selected and adjacent rays are added. If the selected pair is close to the border of the section the adjacent rays are added from only one side.

## V. EXPERIMENTS

A simulation study is conducted to show how the different selection strategies UNI, GAR and LDM, performs with regard to the precision in the position estimate. The strategies are also compared to the case of using all available measurements without selection.

### A. Setup

The two horizontally mounted lidars in total produce 362 laser measurements in each scan, 60 of them are selected for processing. With the GAR strategy, 6 rays are selected according to the greedy approach and then 9 adjacent rays are included. In the LDM strategy, each observable half disc of the lidars is split into 3 sections, where the pair with largest numerical derivative is selected and then adjacent rays are added.

Simulations are performed with two different maps covering the same operational area. One is created from real sensor data and the other one is a synthetic version with straight walls, referred to as the *realistic* and *simplified* map, respectively. Laser scans are simulated by geometrically calculating the ranges from the lidar position to the wall and then add white Gaussian noise with standard deviation 35 mm according to the specification of the physical Lidar (sick LMS500 series).

In the operation area, four vehicle poses with different conditions for position estimation have been chosen where one measurement update of the UKF is performed, see Fig. 5. Pose A is in the middle of a long tunnel, far away from corners that can give a high value of  $\nabla_x s$ , which makes this pose hard from a positioning point of view. At least in the  $x$ -direction. In Pose B a T-junction is present just ahead of the vehicle, which puts a few points with large  $\nabla_x s$  into the field of view of the lidar. In Pose C and D the vehicle is placed in the middle of a cross-section where a lot of informative points/regions in

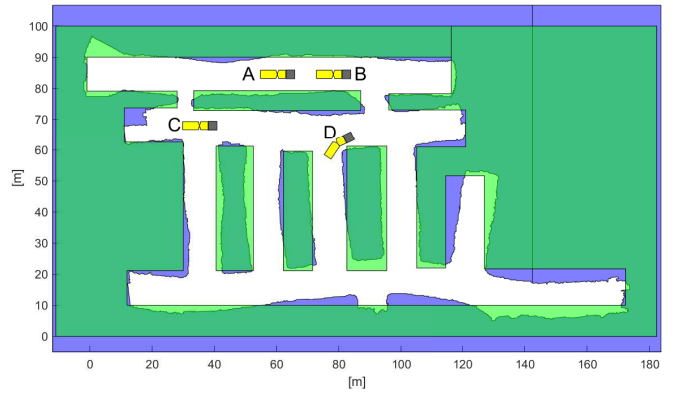


Fig. 5. Different poses considered for one measurement update of the UKF. The two maps are overlaid with the simplified map in green and the realistic map in blue.

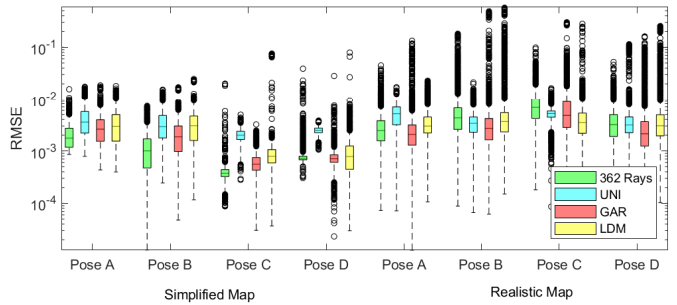


Fig. 6. The RMSE from 10000 realizations when one measurement update is performed for different selection strategies of laser measurements. See Fig. 5 for the vehicle poses A, B, C and D. The edges of the boxes indicates 25th and 75th percentiles, and the median is marked with a horizontal line. The whiskers extend to the most extreme data points not considered outlier, and outliers are marked individually with a circle.

the map is visible in the sensor measurements. This situation is easier with regards to the position estimation, but is more complex for the selection strategies to prioritize what regions are most important.

The UKF is tuned as  $\alpha = 0.8$ ,  $\beta = 2$ ,  $\kappa = 0$  and the measurement noise covariance is,  $\mathbf{R} = 0.035^2 \mathbf{I}$ . The values of  $\beta$  and  $\kappa$  are commonly used standard values, while the value for  $\alpha$  is non-standard, tuned for this particular application by prior experiments.

The initial pose is perturb with a prior uncertainty with covariance

$$P_0 = \begin{bmatrix} 10^{-4} & 0 & 0 \\ 0 & 10^{-4} & 0 \\ 0 & 0 & 10^{-6} \end{bmatrix}, \quad (26)$$

intended to reflect the desired precision in the state estimate. The precision on the heading is in accordance with the desired translational precision on the rear corner of the vehicle.

### B. Simplified Map

Fig. 6 shows the *root mean square error* (RMSE) of the state vector after the correction is performed in the simplified

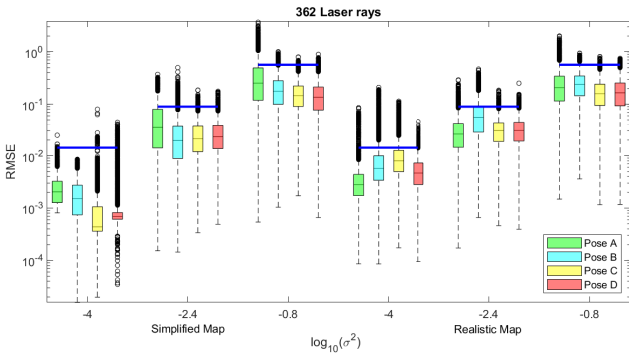


Fig. 7. The RMSE when one correction step is performed in the different poses, when the prior uncertainty,  $P_0 = \sigma^2 \begin{pmatrix} 1 & 0 & 0 \\ 0 & 1 & 0 \\ 0 & 0 & 0.1745^2 \end{pmatrix}$  is increased. The blue horizontal lines are  $\sqrt{\text{tr}(P_0)}$  for each value of  $\sigma^2$ . All 362 available laser measurements are used.

map. For Pose A, the GAR strategy outperforms the other strategies, and in Pose B this is even more emphasized. In Pose C and D where a lot of corners are present LDM, and GAR gives far better results than the UNI strategy. They are even at the same order of magnitude as when all 362 rays are processed. Since the LDM strategy is computationally cheap compared to the GAR strategy, it is worth noting that they perform equally when there is a lot of information in the map. When the information is sparser in the map, LDM performs worse.

### C. Realistic Map

Fig. 6 also shows the results from the same simulation setup applied on the realistic map. As for the simplified map, in general GAR is the best performing strategy. For Pose C and D the RMSE for all strategies are higher than for the simplified map, which means that the pose estimate cannot take advantage of the irregularities of the walls. Not even when using all 362 rays. The relatively large value of  $\alpha$  can cause the filter to smooth out the irregularities. Or, the uncertainty in the pose causes the ray to hit the wrong small feature. In the realistic map the irregularities of the walls are on the order of decimeters, and  $P_0$  is in the order of centimeters. But (20) together with the results in Fig. 7 where the correction step is performed with increasing prior uncertainty in the state vector, indicates that this is not enough. If it were, the RMSE would be smaller in the realistic map compared to the simplified when the prior uncertainty is decreased. The heading component in (20) describes how  $\nabla_{\mathbf{x}}s$  gets larger in magnitude for long range measurements with small inclination angles, which means the measurements with these characteristics have a good potential of being informative. But, if  $\nabla_{\mathbf{x}}s$  is larger than the irregularities of the walls, these measurements will give false information since they hit the wrong irregularity. The risk to encounter this effect increases for long range measurements with small inclination angles.

Fig. 8 depicts how the rays are selected in Pose **D** for the different selection strategies. The GAR strategy selects fewer

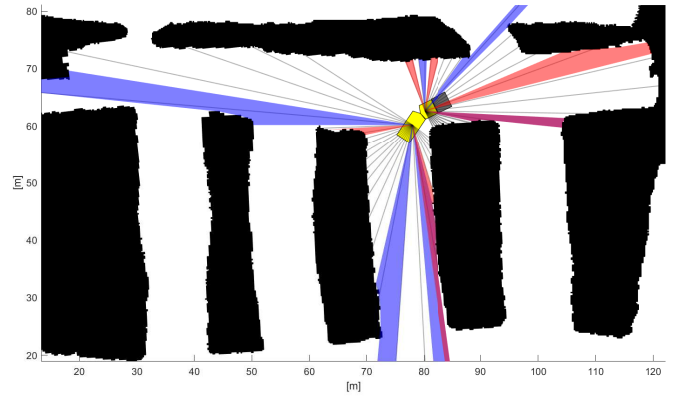


Fig. 8. The selected rays for different strategies are visualized for Pose **D**. Grey lines are UNI, red is GAR and blue is LDM. The purple fields are when GAR and LDM strategies overlaps.

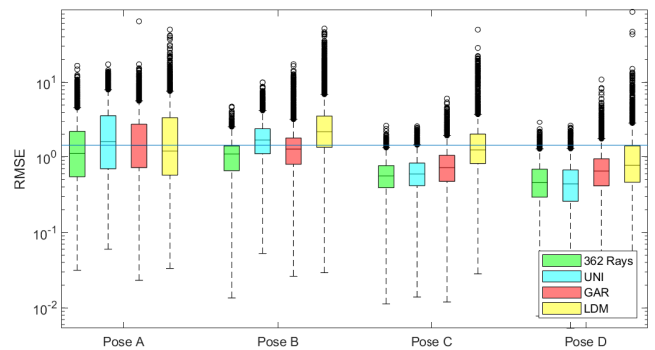


Fig. 9. The RMSE when one correction step is performed with laser data simulated in the realistic map and the estimation done in the simplified map. The prior uncertainty,  $P_0 = \begin{pmatrix} 1 & 0 & 0 \\ 0 & 1 & 0 \\ 0 & 0 & 0.1745^2 \end{pmatrix}$ . The blue horizontal line is  $\sqrt{\text{tr}(P_0)}$ .

long range measurement than the LDM strategy and that is probably why it performs better in this situation.

There is an interesting situation in Pose B and C where using all 362 rays are worse than any of the selection strategies. Since this cannot be seen in the simplified map this is probably also an effect of the rays hitting the wrong irregularity.

### D. Map with Errors

To simulate a scenario of a map with errors, now consider the realistic map as a perfect representation of the walls, and the simplified map is the only available map. Lidar observations are simulated from the realistic map and the position estimation is performed in the simplified map, see Fig. 9 for results. To get the estimated pose to be more accurate after the correction step than before,  $P_0$  had to be increased to meter precision for this simulation. That is not surprising since the errors in the map are of this order of magnitude.

The LDM strategy performs poorly when there are errors in the map. Regions/points of interest that are captured in the observed data are simply not present in the map. That is

according to the results worse than the opposite, choose points of interest in the map and then receive measurements that are not corresponding, as is the case for the GAR strategy. But neither LDM nor GAR are significantly better than the UNI strategy when this type of errors are present in the map.

## VI. CONCLUSION

The demand of robust, highly accurate, infrastructure-free positioning systems for the underground mining industry is complicated by real-time requirements and limited computational resources. In this work we have shown the possibility to reduce computational complexity while preserving quality in a 2D lidar-based position estimate by cleverly selecting a subset of laser measurements.

By analyzing the information contribution of each laser ray measurement, expressions were derived that separates the contribution from the map geometry itself and the relative sensor position. The expressions expose a contradiction for long range measurements with small inclination angles. These are potentially the most informative measurements, but on the same time the measurements with largest error. Especially in maps with high resolution of irregularities of the wall, there is a risk that the laser ray hits the wrong feature in the map due to prior uncertainty of the position. Additionally, in case of an imperfect map the features might not even be present.

The information analysis indicated which ray measurements are informative and have been used to develop two selection strategies. One is based on map geometry and the other one on observed data. Simulation experiments have shown an improvement in accuracy of the position estimate compared to the baseline strategy of uniformly selecting laser rays for both strategies. The strategy based on map geometry performed slightly better than the one based on observed data, but the latter required less computational resources. In the situation of a flawed map, simulations indicate that the developed strategies lose performance. Future work will therefore target the issue of finding strategies that robustly handles imperfections in a map.

## REFERENCES

- [1] L. Thrybom, J. Neander, E. Hansen, and K. Landernas, "Future challenges of positioning in underground mines," in *Proc. 2<sup>nd</sup> IFAC Conf. on Embedded Systems, Computer Intelligence and Telematics CESCIT*, vol. 48, no. 10, Maribor, Slovenia, 2015, pp. 222–226.
- [2] U. Artan, J. A. Marshall, and N. J. Lavigne, "Robotic mapping of underground mine passageways," *Mining Technology*, vol. 120, no. 1, pp. 18–24, 2011.
- [3] J. Paraszczak, A. Gustafson, and H. Schunnesson, "Technical and operational aspects of autonomous LHD application in metal mines," *International Journal of Mining, Reclamation and Environment*, vol. 29, no. 5, pp. 391–403, 2015.
- [4] H.-J. Kwak, D.-H. Lee, J.-M. Hwang, J.-H. Kim, C.-K. Kim, and G.-T. Park, "Improvement of the inertial sensor-based localization for mobile robots using multiple estimation windows filter," in *Proc. IEEE/RSJ Int. Conf. on Intelligent Robots and Systems*, Vilamoura, Portugal, 2012, pp. 876–881.
- [5] C. A. Niestroj, C. Niedringhaus, and K. Nienhaus, "Development of an underground positioning system based on the ultra-wideband radio technology," *Mining report*, vol. 153, no. 1, pp. 69–76, 2017.
- [6] G. Jekabsons, V. Kairish, and V. Zuravlyov, "An analysis of wi-fi based indoor positioning accuracy," *Scientific Journal of Riga Technical University. Computer Science*, vol. 44, no. 1, pp. 131–137, 2011.
- [7] H. Liu, H. Darabi, P. Banerjee, and J. Liu, "Survey of wireless indoor positioning techniques and systems," *IEEE Trans. Syst., Man, Cybern. C*, vol. 37, no. 6, pp. 1067–1080, 2007.
- [8] R. Mautz, "The challenges of indoor environments and specification on some alternative positioning systems," in *Proc. 6<sup>th</sup> Workshop on Positioning, Navigation and Communication*, Hannover, Germany, 2009, pp. 29–36.
- [9] M. A. Al-Ammar, S. Alhadhrami, A. Al-Salman, A. Alarifi, H. S. Al-Khalifa, A. Alnafessah, and M. Alsaleh, "Comparative survey of indoor positioning technologies, techniques, and algorithms," in *Proc. Int. Conf. on Cyberworlds*, Santander, Spain, 2014, pp. 245–252.
- [10] A. Chehri, P. Fortier, and P. M. Tardif, "UWB-based sensor networks for localization in mining environments," *Ad Hoc Networks*, vol. 7, no. 5, pp. 987–1000, 2009.
- [11] J. C. Ralston, C. O. Hargrave, and D. W. Hainsworth, "Localisation of mobile underground mining equipment using wireless ethernet," in *40<sup>th</sup> IAS Annual Meeting. Conf. Record of the Industry Applications Conf.*, vol. 1, Kowloon, Hong Kong, China, 2005, pp. 225–230.
- [12] M. Cypriani, G. Delisle, and N. Hakem, "Wi-Fi-based positioning in a complex underground environment," *Journal of Networks*, vol. 10, no. 3, 2015.
- [13] A. Yassin, Y. Nasser, M. Awad, A. Al-Dubai, R. Liu, C. Yuen, R. Raulefs, and E. Aboutanios, "Recent advances in indoor localization: A survey on theoretical approaches and applications," *IEEE Commun. Surveys Tuts.*, vol. 19, no. 2, pp. 1327–1346, 2017.
- [14] A. E. Assaf, S. Zaidi, S. Affes, and N. Kandil, "Accurate sensors localization in underground mines or tunnels," in *Proc. IEEE Int. Conf. on Ubiquitous Wireless Broadband (ICUWB)*, Montreal, QC, Canada, 2015, pp. 1–6.
- [15] H. Chi, K. Zhan, and B. Shi, "Automatic guidance of underground mining vehicles using laser sensors," *Tunnelling and Underground Space Technology*, vol. 27, no. 1, pp. 142–148, 2012.
- [16] G. W. Ng and K. H. Ng, "Sensor management – what, why and how," *Information Fusion*, vol. 1, no. 2, pp. 67–75, 2000.
- [17] A. O. Hero and D. Cochran, "Sensor management: past, present, and future," *IEEE Sensors J.*, vol. 11, no. 12, pp. 3064–3075, 2011.
- [18] S. Joshi and S. Boyd, "Sensor selection via convex optimization," *IEEE Trans. Signal Process.*, vol. 57, no. 2, pp. 451–462, 2009.
- [19] S. P. Chepuri and G. Leus, "Sparsity-promoting sensor selection for non-linear measurement models," *IEEE Trans. Signal Process.*, vol. 63, no. 3, pp. 684–698, 2015.
- [20] S. Rao, S. P. Chepuri, and G. Leus, "Greedy sensor selection for non-linear models," in *Proc. IEEE 6<sup>th</sup> Int. Workshop on Computational Advances in Multi-Sensor Adaptive Processing (CAMSAP)*, Cancun, Mexico, 2015, pp. 241–244.
- [21] H. Zhang, R. Ayoub, and S. Sundaram, "Sensor selection for Kalman filtering of linear dynamical systems: complexity, limitations and greedy algorithms," *Automatica*, vol. 78, pp. 202–210, 2017.
- [22] M. Shamaiah, S. Banerjee, and H. Vikalo, "Greedy sensor selection: leveraging submodularity," in *Proc. 49<sup>th</sup> IEEE Conf. on Decision and Control (CDC)*, Atlanta, GA, USA, 2010, pp. 2572–2577.
- [23] D. Nitzan, A. E. Brain, and R. O. Duda, "The measurement and use of registered reflectance and range data in scene analysis," *Proc. IEEE*, vol. 65, no. 2, pp. 206–220, 1977.
- [24] S. J. Julier, J. K. Uhlmann, and H. F. Durrant-Whyte, "A new method for the nonlinear transformation of means and covariances in filters and estimators," *IEEE Trans. Autom. Control*, vol. 45, no. 3, 2000.
- [25] S. Särkkä, *Bayesian filtering and smoothing*, ser. Institute of Mathematical Statistics Textbooks. Cambridge University Press, 2013.
- [26] E. A. Wan and R. V. D. Merwe, "The unscented Kalman filter for nonlinear estimation," in *Proc. IEEE Adaptive Systems for Signal Processing, Communications, and Control Symp. (Cat. No.00EX373)*, Lake Louise, Alberta, Canada, 2000.
- [27] R. Van der Merwe and E. A. Wan, "The square-root unscented Kalman filter for state and parameter-estimation," in *Proc. 2001 IEEE Int. Conf. on Acoustics, Speech, and Signal Processing (Cat. No.01CH37221)*, vol. 6, Salt Lake City, UT, USA, 2001, pp. 3461–3464.
- [28] S. M. Kay, *Fundamentals of statistical signal processing - estimation theory*. Prentice Hall, 1993.
- [29] P. Tichavsky, C. H. Muravchik, and A. Nehorai, "Posterior Cramer-Rao bounds for discrete-time nonlinear filtering," *IEEE Trans. Signal Process.*, vol. 46, no. 5, pp. 1386–1396, 1998.